Structural, morphological, optical and electrical properties of Al-doped ZnO thin films prepared by Sol-Gel spin coating

A. Carrero[a,b,c,*], P. Perillo[a,b], D. Rodríguez[a,b], and M. Barrera[a,b,c]

[a]*Comisión Nacional de Energía Atómica, Centro Atómico Constituyentes, e-mail: aneelyc@gmail.com*

[b]*Instituto de Nanociencia y Nanotecnología, CNEA–CONICET,*

[c]*Departamento Energía Solar, CAC–CNEA.*

Received 17 April 2026; accepted 4 August 2026

Undoped and aluminum-doped ZnO (AZO) thin films were prepared by the sol-gel method using spin coating. The films exhibited the characteristic wurtzite crystal structure of ZnO with a preferential orientation along the c-axis. Surface and cross-sectional morphologies were analyzed by scanning electron microscopy (SEM), revealing noticeable differences between the doped and undoped films. The optical transmittance was approximately 77% in the 450-750 nm range. Electrical resistivity decreased from 1.9×10^5 Ω·cm (ZnO) to 1.0×10^2 Ω·cm (AZO). These results suggest that low-level Al doping enhances the electrical properties while preserving good optical transparency in AZO thin films. Furthermore, the results highlight the correlation between structural, optical, and electrical properties in ZnO and AZO thin films.

Keywords: Al-Doped ZnO; Sol–Gel; spin coating technique; structural properties; optical transparency.

DOI: https://doi.org/10.31349/RevMexFis.72.061005

1. Introduction

Zinc oxide (ZnO) is a II-VI semiconductor with a wide direct band gap of approximately 3.37 eV at room temperature. In addition, it exhibits a high exciton density due to its large exciton binding energy (60 meV). ZnO is also characterized by high optical transparency in the visible and near-ultraviolet regions, highlighting its strong potential for optoelectronic applications [1-3]. Furthermore, ZnO has been extensively investigated for applications in photocatalysis [4], piezoelectric devices [5], solar cells [6], and as a transparent conductive contact [7-8]. The electrical, optical, and morphological properties of ZnO can be tailored through doping [2,6]. In this material, doping can be achieved by substituting cationic sites Zn^{2+} with metals or anionic sites O^{2-} with non-metals [6,9]. In particular, doping with group III elements, such as Al, Ga, or In, has proven to be an effective strategy for enhancing the electrical properties of ZnO. AZO thin films exhibit increased electrical conductivity while maintaining high optical transmittance, making them attractive candidates for transparent electronics applications [1]. Moreover, AZO thin films stand out due to their thermal stability, low cost, and excellent transparency, which make them especially suitable for electro-optical applications [10-11] Various deposition techniques have been employed to fabricate AZO films, including pulsed laser deposition [12-13], molecular beam epitaxy (MBE) [14], and RF or DC magnetron sputtering [15-16]. However, these methods typically require complex and expensive equipment. On the other hand, AZO films can be synthesized using the sol-gel method, which has attracted significant attention due to its simplicity, low cost, and potential for large-area coating [2,17-18]. Moreover, the structural, optical, and electrical properties of the resulting films are strongly influenced by several parameters, such as the substrate, solvent, annealing temperature, doping concentration, aging time, and precursor molar concentration [2,19-21]. On the other hand, obtaining AZO films with preferential orientation along the c-axis prepared by the sol-gel method is a challenge due to the various processing parameters. AZO films with preferential orientation are of great interest for applications in photovoltaic or optoelectronic devices [18,22-23]. In this work, ZnO and AZO thin films with preferential orientation along the c-axis were prepared by a sol-gel spin-coating route and deposited onto glass substrates. The films were comparatively analyzed in terms of their structural, morphological, optical, and electrical properties. This study aims to provide further insight into the effect of low aluminum concentration on the properties of ZnO thin films, contributing to a better understanding of how subtle compositional modifications influence their performance and potential application in optoelectronic devices.

2. Materials and methods

2.1. Preparation of ZnO and Al-Doped ZnO precursor sols

Undoped ZnO and aluminum-doped ZnO sols were synthesized via the sol-gel method. Zinc acetate dihydrate ($Zn(CH_3COO)_2{\cdot}2H_2O$) was used as the zinc precursor, absolute ethanol as the solvent, monoethanolamine (MEA) as the stabilizing agent, and aluminum nitrate nonahydrate ($Al(NO_3)_3{\cdot}9H_2O$) as the dopant source. For the AZO sols, aluminum was introduced at a nominal concentration of 0.8

at%. A 0.2 M solution was prepared by dissolving 0.02 mol of zinc acetate in 100 mL of ethanol. While the solution was stirred and heated to 80°C, MEA was added dropwise at a fixed MEA:Zn molar ratio of 1:1, inducing a transition from a whitish to a transparent solution. Subsequently, aluminum nitrate was added, and the mixture was refluxed for 3 h. Finally, the resulting sol was aged for 48 h prior to thin-film deposition.

2.2. Thin-film deposition and thermal treatment

Thin films were deposited onto cover glass substrates by spin coating. Prior to deposition, the substrates were sequentially cleaned with acetone, isopropyl alcohol, and deionized water, and then dried under a nitrogen stream. Spin coating was carried out at 2000 rpm for 40 s. After each coating step, the films were preheated on a hot plate at 100°C for 10 min to promote solvent evaporation and remove residual organic species. This coating-drying cycle was repeated six times to obtain the desired film thickness. Finally, the films were annealed in a furnace at 500°C for 2 h with a heating rate of 5°C/min and then allowed to cool naturally to room temperature.

The deposition conditions were optimized, and the films reported here were obtained under these optimized, controlled, and reproducible parameters.

2.3. Film characterization

The crystallinity of the films was analyzed by X-ray diffraction (XRD) using a Panalytical Empyrean diffractometer operating in parallel-beam geometry with CuKα radiation. Surface and cross-sectional morphologies were examined by scanning electron microscopy (SEM) using a Carl Zeiss Supra 40 Gemini microscope. Optical properties were characterized by UV–Vis spectroscopy using a GBC UV–Vis 920 spectrophotometer. Electrical resistance was measured using the standard four-point probe technique.

3. Results and discussion

3.1. Structural and morphology of the films

Figure 1 shows the X-ray diffraction (XRD) patterns of undoped ZnO and Al-doped ZnO films grown on cover glass. The crystalline planes present in the films were identified using Miller indices (*hkl*). The diffraction peaks match well with the JCPDS PDF card No. 00-036-1451, confirming that the films exhibit the typical wurtzite structure of ZnO, are polycrystalline, and show a preferential orientation along the (002) direction. Moreover, no additional crystalline phases, such as aluminum oxide or other impurities, were detected.

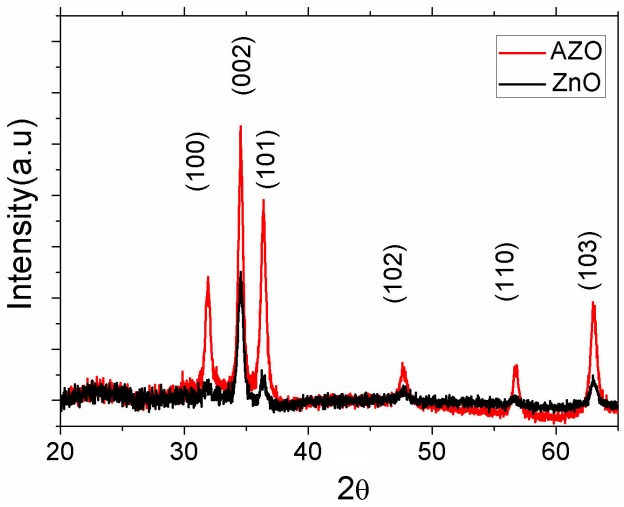


FIGURE 1. XRD patterns of undoped and Al-doped ZnO thin films.

The lattice parameters were calculated from the diffractogram using the following relations [24-26]:

$$\frac{1}{d_{hkl}^2} = \frac{4}{3}\left(\frac{h^2+hk+k^2}{a^2}\right) + \frac{l^2}{c^2}, \tag{1}$$

$$d_{hkl} = \frac{\lambda}{2\sin\theta}, \tag{2}$$

where d_{hkl} denotes the interplanar spacing for the (hkl) planes, and a and c represent the lattice constants. The calculated lattice parameters for the undoped ZnO and AZO films are presented in Table I. No significant changes in the lattice parameters are observed after Al incorporation, which can be attributed to the relatively low aluminum concentration used in this work. This behavior is consistent with previous reports on doped ZnO films [2,21]. Moreover, the c/a ratio is in agreement with the typical value for ZnO, confirming the hexagonal wurtzite crystal structure of the films. The crystallite size was estimated using the Debye-Scherrer equation [21,27-28], employing the full width at half maximum (FWHM) of the most intense diffraction peak (see Table I). The larger crystallite size observed for the doped film suggests that Al incorporation may have modified the growth kinetics, possibly through enhanced atomic mobility, reduced grain boundary energy, and decreased microstrain and defect density.

TABLE I. Crystallite size (D), lattice constants (a, c), and c/a ratio of ZnO and AZO films determined from XRD analysis.

Parameter	ZnO	AZO
$a = b$ (Å)	3.242 (2)	3.242 (4)
c (Å)	5.191 (1)	5.191 (6)
c/a	1.601	1.601
D (nm)	10.6 (3)	17.0 (7)

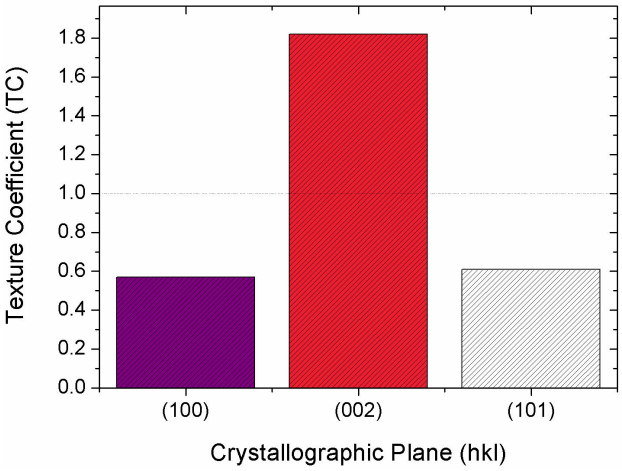


FIGURE 2. Texture coefficients of the (100), (002), and (101) planes of the AZO thin film.

In order to examine the preferred orientation of the crystal structure, the texture coefficient (TC) was calculated from the XRD data using the following equation [2,21,27-28]:

$$TC_{\text{hkl}} = \frac{I_{(\text{hkl})}/I_{0(\text{hkl})}}{\frac{1}{N}\sum_n \left(I_{(\text{hkl})}/I_{0(\text{hkl})}\right)}, \tag{3}$$

where $I_{(\text{hkl})}$ is the measured intensity of the (hkl reflection and $I_0(\text{hkl})$ is the corresponding standard intensity and N is the number of diffraction peaks considered. A $TC > 1$ indicates preferential growth of the film along the corresponding crystallographic plane.

In Fig. 2 the texture coefficient (TC) values indicate that the AZO film exhibits preferential growth along the (002) crystallographic plane $(TC_{002} = 1.82)$, consistent with the XRD diffractogram. This preferential orientation along the c-axis indicates a higher degree of crystallographic alignment and may favor the development of more ordered crystalline domains. This structural feature can contribute to the functional properties of the AZO film, including its electrical performance.

The SEM images of the surface of undoped and aluminum-doped ZnO thin films are shown in Fig. 3a) and 3b), respectively. The undoped ZnO film exhibits a porous morphology with a granular structure and an average grain size of approximately 40 nm. In contrast, the AZO film displays a denser and more homogeneous surface, consisting of grains with an average size of about 49 nm, as determined from the micrograph analysis using ImageJ software.

The cross-sectional SEM images are shown in Figs. 3c) - 3d). Both thin films exhibit a granular structure [29], and the grains display a preferred growth orientation, as they are not completely spherical [30-31]. This observation is consistent with the preferential growth inferred from the XRD analysis. The undoped ZnO film appears less homogeneous, with higher surface roughness and a less densely packed structure compared to the Al-doped ZnO film, suggesting that the dopant plays a significant role in influencing the film morphology [2,6]. The film thicknesses estimated from the cross-sectional SEM images were approximately 170 nm for the undoped ZnO film and 163 nm for the AZO film.

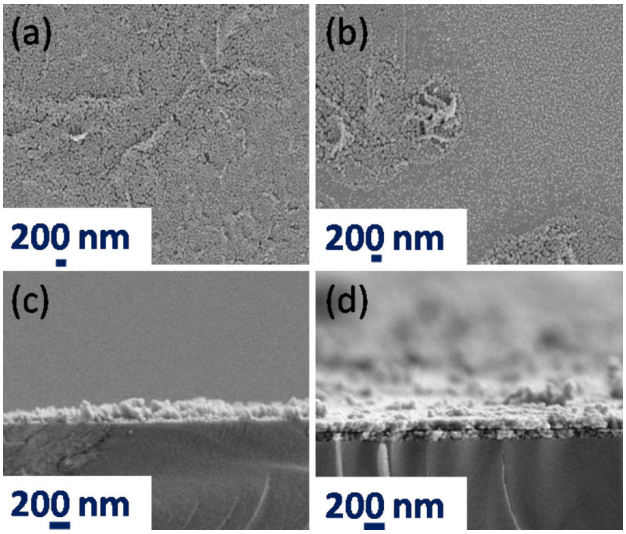


FIGURE 3. SEM top-view images of undoped ZnO a) and AZO b), and cross-sectional images of undoped ZnO c) and AZO d) films on cover glass substrates.

3.2. Optical characterization

Figure 4 shows the transmittance spectra of the undoped ZnO film, the Al-doped ZnO film, and the glass coverslip substrate. Two main features can be identified in the spectra. First, the absorption edge of both ZnO films (undoped and Al-doped) appears around 390 nm, which is associated with the fundamental band-to-band transition of ZnO. Additionally, a shoulder with a maximum around 330 nm is observed in the UV region. Second, in the visible region (450–750 nm), the undoped ZnO film exhibits an average transmittance of approximately 94%, slightly higher than that of the glass coverslip substrate (∼92%). This behavior could be

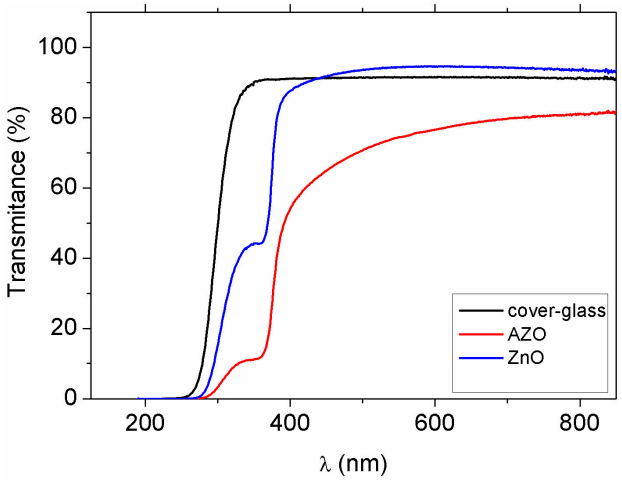


FIGURE 4. Transmittance spectra of undoped ZnO, AZO thin films and the cover glass substrate.

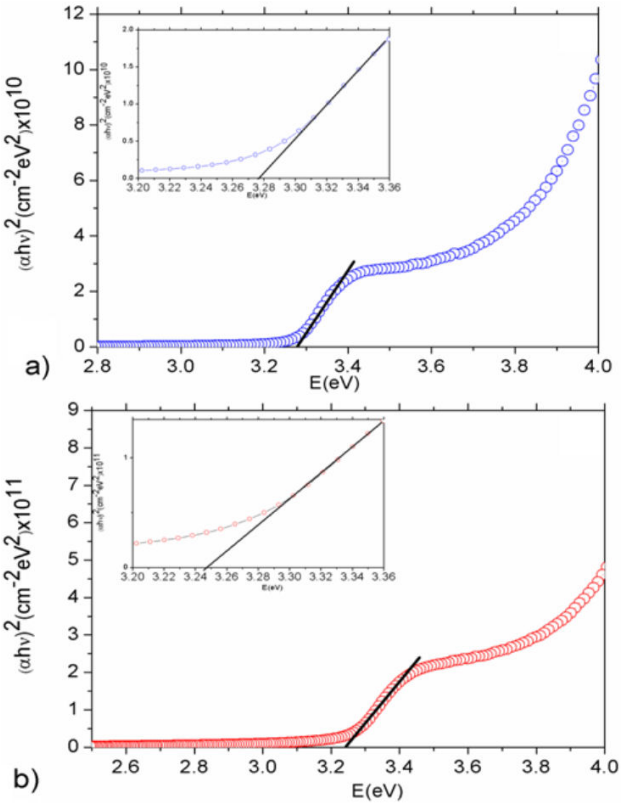


FIGURE 5. Optical band gap energy of undoped ZnO a) and AZO b) thin films.

be related to the thickness of the ZnO film ($\approx$ 170 nm, estimated from SEM images), which is close to the optical optimum for antireflection conditions, as well as to its morphology characterized by the presence of voids, which may promote a partial antireflection effect in the air/film/glass system [32-33]. In contrast, the Al-doped ZnO film shows a lower transmittance (77%) in the visible range (450–750 nm). This difference may be associated with the more compact and homogeneous morphology of the AZO film compared with the undoped ZnO film, as revealed by the SEM images [Fig. 3c) and 3d)] [33,34-36].

The energy band gap value was determined from transmittance measurements. The optical absorption coefficient was calculated using the Beer-Bouguer-Lambert law, according to the expression $\alpha = -(1/d)\ln(T)$, where d is the thickness of the film [37-39]. The energy gap of the films was estimated by using the Tauc relation [40-41], given by: $\alpha h\nu = A(h\nu - Eg)^{1/2}$, Where $h\nu$ is the photon energy, α is the absorption coefficient, Eg is the band gap energy and A is a constant. Fig. 5 shows that the band gap energy was determined by extrapolating the straight line of the curve to the point where $(\alpha h\nu)^2 = 0$. The obtained values were 3.28 eV and 3.24 eV for the undoped and doped ZnO films, respectively. The slight reduction in the optical band gap may be attributed to Al incorporation, which can introduce shallow donor states near the conduction band as well as defect- or disorder-related states within the band gap [10,41]. These

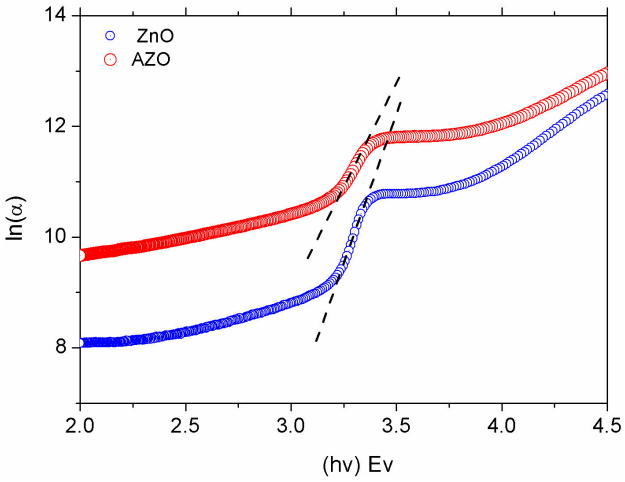


FIGURE 6. $\ln(\alpha)$ versus photon energy for undoped ZnO and AZO thin films.

effects can lead to band tailing and a shift of the absorption edge toward lower energies, as will be further discussed in relation to the Urbach energy analysis. Although Al doping is often associated with increased carrier concentration and a Burstein-Moss shift leading to an apparent band gap widening, the observed behavior suggests that band-gap narrowing mechanisms dominate in the present case. This may be related to the relatively low Al concentration and the presence of structural disorder or defect states, which can mask the Burstein-Moss effect.

In semiconductors, the optical absorption below the band-edge energy exhibits an exponential behavior, known as the Urbach tail. The energy associated with this tail is referred to as the Urbach energy (Eu) and provides information about the degree of disorder present near the band edge. The Urbach energy can be described by the following relation [42-43]:

$$\alpha = \alpha_0 \exp\left(\frac{h\nu}{E_u}\right), \tag{4}$$

where α_0 is a constant and hν represents the photon energy. The value of Eu was obtained from the plot of the natural logarithm of the absorption coefficient, $\ln(\alpha)$, as a function of the photon energy (hν), as shown in Fig. 6. The linear region of the curve was fitted, and Eu was determined from the inverse of the slope. The obtained values were 102 meV and 207 meV for the undoped ZnO and Al-doped ZnO thin films, respectively, suggesting that the incorporation of Al increases the electronic disorder of the system. These values are in good agreement with those reported for ZnO and AZO thin films in the literature [44-45].

3.3. Electric characterization

The electrical resistivity ρ of the thin films was determined using the relation

$$\rho = \frac{\pi}{\ln 2}\frac{V}{I}t, \tag{5}$$

TABLE II. Main structural, optical, and electrical parameters for ZnO and AZO thin films.

Parameter	ZnO	AZO
Crystallite size (nm)	10.6	17.0
Thickness (nm)	170	163
Transmittance (%) (450-750nm)	94	77
Resistivity ($\Omega \cdot$ cm)	1.9×10^5	1.0×10^2

where $\pi / \ln 2$, is the geometrical correction factor for thin films and t is the film thickness [46]. The resistivity values obtained were $1.9 \times 10^5\,\Omega \cdot$ cm and $1.0 \times 10^2\,\Omega \cdot$ cm for the undoped ZnO and Al-doped ZnO films, respectively. These results indicate that Al doping reduces the resistivity of the ZnO film by approximately three orders of magnitude. Similar resistivity values have been reported for AZO thin films deposited on glass substrates by the sol-gel method [3,23,47]. This decrease in resistivity suggests that Al incorporation modifies the electrical properties of ZnO, possibly through donor-like behavior. A commonly proposed mechanism is the substitution of Zn^{2+} by Al^{3+} ions acting as donor centers [3]. However, in the absence of direct evidence of substitution Al incorporation (*e.g.*, Hall-effect measurements or compositional analysis), this interpretation should be regarded as plausible rather than definitive. Additionally, the improved crystallinity and denser morphology of the doped films may also contribute to the enhanced electrical conductivity [39,43].

A summary about the main results is presented in Table II.

4. Conclusions

ZnO and AZO thin films with a nominal Al concentration of 0.8 at.% were successfully prepared by the sol-gel method using spin coating. The films exhibit the characteristic wurtzite crystal structure of ZnO, are polycrystalline and show a preferential c-axis orientation, with improved structural ordering observed upon Al incorporation.

SEM analysis revealed that the AZO film is more uniform, denser, and compact than the undoped ZnO film. The optical transmittance of the AZO film is approximately 77% in the visible range (450-750 nm), being lower than that of the undoped ZnO film. A slight decrease in the optical band gap was observed, from 3.28 eV for ZnO to 3.24 eV for AZO. A significant decrease in electrical resistivity was observed, $1.9 \times 10^5\,\Omega \cdot$ cm (ZnO) to $1.0 \times 10^2\,\Omega \cdot$ cm (AZO).

In summary, ZnO and AZO thin films were obtained using a simple and low-cost method. The results show that Al doping leads to a significant improvement in the electrical properties while maintaining good optical transparency. These results provide further insight into the effect of low-level Al doping on ZnO thin films by correlating their structural, morphological, optical, and electrical properties and support their potential use in optoelectronic applications.

Acknowledgments

This work was financed by the Argentine National Atomic Energy Commission (CNEA), the Argentinian National Council for Scientific and Technical Research (CONICET) and the National Agency for Scientific and Technological Promotion (ANPCyT) through grant PICT-2021-I-A-00206. The authors gratefully acknowledge the Crystallography Group at CNEA for their support. In particular, we thank Diego Lionello and Daniel Vega for their collaboration in carrying out the crystallographic measurements.

1. Z. Wang *et al*., Vacancy cluster in ZnO films grown by pulsed laser deposition, *Sci. Rep.* **9** (2019) 3534, https://doi.org/10.1038/s41598-019-40029-3.
2. T. Ivanova *et al*., Sol-Gel synthesis of ZnO:Li thin films: Impact of annealing on structural and optical properties, *Crystals* **14** (2023) 6, https://doi.org/10.3390/cryst14010006.
3. S. Mridha, D. Basak, Aluminium doped ZnO films: electrical, optical and photoresponse studies, *J. Phys. D: Appl. Phys.* **40** (2007) 6902, https://doi.org/10.1088/0022-3727/40/22/008.
4. K. M. Mohamed *et al*., Recent advances in ZnO-based nanostructures for photocatalytic degradation, *Crystals* **13** (2023) 329, https://doi.org/10.3390/cryst13020329.
5. S. Ghosh *et al*., Piezoelectric-based bioactive ZnO-cellulose acetate mats, *Front. Immunol.* **14** (2023) 1245343, https://doi.org/10.3389/fimmu.2023.1245343.
6. A. Wibowo *et al*., ZnO nanostructured materials for solar cell applications, *RSC Adv.* **10** (2020) 42838, https://doi.org/10.1039/D0RA07689A.
7. N. Zhang *et al*., ZnO transparent conductive films with upconversion function, *Mater. Sci. Eng. B* **325** (2026) 119076, https://doi.org/10.1016/j.mseb.2025.119076
8. Y. C. Kao *et al*., Performance comparison of III-V multijunction solar cells, *Sci. Rep.* **9** (2019) 4308, https://doi.org/10.1038/s41598-019-40727-y.
9. D. Zhao *et al*., n-Type conducting P-doped ZnO thin films, *RSC Adv.* **10** (2020) 34527, https://doi.org/10.1039/D0RA05667G.
10. I. Jellal *et al*., Comparative study of Al- and Nidoped ZnO films, *Opt. Quantum Electron.* **55** (2023) 620, https://doi.org/10.1007/s11082-023-04798-6.

11. L. E. Morinigo *et al*., Aluminum-doped zinc oxide thin films, *Mater. Sci. Eng. B* **318** (2025) 118279, https://doi.org/10.1016/j.mseb.2025.118279.
12. Q. A. Drmosh *et al*., Cu-doped ZnO thin films by PLD, *Appl. Surf. Sci.* **270** (2013) 104, https://doi.org/10.1016/j.apsusc.2012.12.126.
13. N. K. Temizer *et al*., Ferromagnetism in Al-doped ZnO films, *AIP Adv*. **14** (2024) 105331, https://doi.org/10.1063/5.0224007.
14. L. He *et al.*, Topological insulator thin films, *Phys. Status Solidi RRL* **7** (2013) 50, https://doi.org/10.1002/pssr.201307003.
15. Y. Shen *et al*., Blue light emission from ZnO/GaN heterojunction, *Curr. Appl. Phys*. **14** (2014) 345, https://doi.org/10.1016/j.cap.2013.12.011.
16. W. Yang *et al*., Al-doped ZnO films by sputtering, *Appl. Surf. Sci.* **255** (2009) 5669, https://doi.org/10.1016/j.apsusc.2008.12.021.
17. Y. Ammaih *et al*., ZnO:Al thin films properties, Opt. Quantum Electron. **46** (2014) 229, https://doi.org/10.1007/s11082-013-9757-2.
18. X. Zi-qiang *et al*., Al-doping effects in ZnO films, *Mater. Sci. Semicond. Process.* **9** (2006) 132, https://doi.org/10.1016/j.mssp.2006.01.082.
19. H. M. Hussein, Cu-doped ZnO thin films, *Results Opt*. **13** (2023) 100543, https://doi.org/10.1016/j.rio.2023.100543.
20. H. Stroescu *et al*., Sol-gel AZO thin films, *Materials* **16** (2023) 3329, https://doi.org/10.3390/ma16093329.
21. K. D. A. Kumar *et al.*, Sol-gel Al-doped ZnO films, *Appl. Phys. A* **123** (2017) 801, https://doi.org/10.1007/s00339-017-1426-z.
22. K. Baba *et al*., ZnO films by spray plasma, *Thin Solid Films* **595** (2015) 129, https://doi.org/10.1016/j.tsf.2015.10.072.
23. D. Zhang *et al*., Al-doped ZnO films, *J. Am. Ceram. Soc*. **93** (2010) 3291, https://doi.org/10.1111/j.1551-2916.2010.03847.x.
24. M. S. Nadeem *et al*., Co, Ni co-doped ZnO nanorods, *Opt. Mater.* **111** (2021) 110606, https://doi.org/10.1016/j.optmat.2020.110606.
25. A. A. Aboud *et al*., Doping effects on ZnO thin films, *RSC Adv.* **9** (2019) 7729, https://doi.org/10.1039/C8RA10599E.
26. B. D. Cullity, S. R. Stock, Elements of X-ray Diffraction, Prentice Hall, Upper Saddle River, NJ (2001).
27. M. S. Nadeem et al., Sr-doped ZnO thin film, *Opt. Mater.* **157** (2024) 116106, https://doi.org/10.1016/j.optmat.2024.116106.
28. A. Kumar, M. I. Ahmad, Role of defects in Al-doped ZnO films, *J. Mater. Sci*. **57** (2022) 7877, https://doi.org/10.1007/s10853-022-07136-5.
29. M. Khiari *et al*., ZnO thin films by liquid deposition, *Coatings* **12** (2022) 65, https://doi.org/10.3390/coatings12010065.
30. R. G. B. Madera *et al*., ZnO thin films using sintered targets, *Physica B* **698** (2025) 416733, https://doi.org/10.1016/j.physb.2024.416733.
31. M.W. Zhu *et al*., Sol-gel ZnO films, *J. Non-Cryst. Solids* **354** (2008) 2416, https://doi.org/10.1016/j.jnoncrysol.2007.10.037.
32. Y. Demirhan, Anti-reflective coatings, Opt. Quantum Electron. **58** (2026) 75, https://doi.org/10.1007/s11082-026-08675-w.
33. W. Li *et al*., Anti-reflection ZnO coatings, *Mater. Lett*. **243** (2019) 108, https://doi.org/10.1016/j.matlet.2019.01.158.
34. Y. Li *et al*., Superhydrophobic coatings, *Chem. Commun*. (2009) 2730, https://doi.org/10.1039/B900804G.
35. S. Salam *et al*., Sol-gel ZnO films, *Thin Solid Films* **529** (2013) 242, https://doi.org/10.1016/j.tsf.2012.10.079.
36. H. Zhou *et al*., Al-doped ZnO films, *Thin Solid Films* **515** (2007) 6909, https://doi.org/10.1016/j.tsf.2007.01.041.
37. K. Shalimova, Physics of Semiconductors, Mir, Moscow (1975).
38. G. L. Kabongo *et al*., Holmium-doped ZnO, *Nanomaterials* **11** (2021) 2611, https://doi.org/10.3390/nano11102611.
39. N. Al-Khalli *et al*., ZnO thin films properties, *Mater. Trans.* **62** (2021) 915, https://doi.org/10.2320/matertrans.MT-M2020350.
40. J. Tauc, Optical properties of amorphous semiconductors, *Mater. Res. Bull*. **3** (1968) 37.
41. A. López-Suárez *et al*., Mn-doped ZnO films, *J. Mater. Sci.*: *Mater. Electron.* **31** (2020), https://doi.org/10.1007/s10854-019-02830-8.
42. M. R. Islam, M. G. Azam, Mg-doped ZnO films, *Surf. Eng.* **37** (2021) 775, https://doi.org/10.1080/02670844.2020.1801143.
43. F. Urbach, Absorption edge in solids, *Phys. Rev.* **92** (1953) 1324, https://doi.org/10.1103/PhysRev.92.1324.
44. R. C. Rai, Urbach tails in ZnO, *J. Appl. Phys*. **113** (2013) 153508, https://doi.org/10.1063/1.4801900.
45. P. Potera et al., Co-doped ZnO films, *Appl. Sci.* **13** (2023) 2701, https://doi.org/10.3390/app13042701.
46. F. M. Smits, Four-point probe method, *Bell Syst. Tech*. J. **34** (1958) 711.
47. K. M. Salman et al., Mg-doped ZnO films, *Opt. Mater*. **158** (2025) 116460, https://doi.org/10.1016/j.optmat.2024.116460.